Quasicontinuous control of a bronze ribbon experiment using time-delay coordinates

A. Schenck zu Schweinsberg, T. Ritz, and U. Dressler

Daimler-Benz AG, Research Institute Frankfurt, Goldsteinstraße 235, D-60528 Frankfurt, Germany

B. Hübinger, R. Doerner, and W. Martienssen

Physikalisches Institut der J.W. Goethe-Universität, Robert-Mayer-Straße 2-4, D-60325 Frankfurt/Main, Germany

We investigate quasicontinuous versions of the Ott-Grebogi-Yorke (OGY) control method in a bronze ribbon experiment using time-delay coordinates for the reconstruction of the attractor. We apply as quasicontinuous control methods the local control method and the minimal expected deviation method. As is known for the original OGY method with time-delay coordinates, values of the control parameter at previous times appear in the linearized dynamics. We discuss two possible ways to derive from this linearization feedback control formulas. These are the extended state space approach and a modified control requirement that demands stabilization not in the next time step but after $w+1$ time steps, where w is the number of preceding parameter dependences of the linearized dynamics. We show theoretically and demonstrate in the experiment that for the quasicontinuous control methods considered in this paper only the modified control requirement shows satisfying results in the control experiment. [S1063-651X(97)01502-X]

I. INTRODUCTION

Since the late 1980s controlling chaotic systems using methods of nonlinear dynamics has become a very popular area of research in the nonlinear dynamics community. The problem of controlling chaos was addressed by Lüscher and Hübler [1], who proposed an open-loop control to force a chaotic system to a desired goal dynamics by adding a specially designed continuous driving force to the system. To calculate this generally aperiodic force in advance a global model of the system has to be available or must be constructed. Another approach is the feedback control of Ott, Grebogi, and Yorke, which we address in this paper. Ott, Grebogi, and Yorke proposed 1990 in [2] to stabilize unstable periodic orbits (UPOs) embedded in a chaotic attractor by tiny time-dependent parameter perturbations. This work has triggered immense research activities to apply feedback control to chaotic systems (see [3] and references therein). One reason for the attractiveness of the Ott-Grebogi-Yorke (OGY) idea is that it is in principle possible to obtain all control values of the feedback loop from a careful analysis of a scalar measurement signal. No global model is required; solely the local dynamics in the vicinity of the unstable orbit has to be extracted from the measurement data.

With respect to the applicability of the OGY control approach to real-world experiments there have been various variations and extensions, e.g. the tracking approach of Schwartz and Triandaf [4] to cope with slowly varying parameters or the simple OPF feedback control [5] to control very fast experimental systems.

In this paper we want to address and combine the two following modifications of the OGY control. First, in the original OGY control approach the control frequency was limited to the frequency of the piercings of the continuous trajectory through the Poincaré section of the UPO, as Ott, Grebogi, and Yorke reduced the stabilization of a continuous UPO to the stabilization of the corresponding UPO of the

Poincaré mapping. For driven systems, which we consider in this paper, where the Poincaré section is naturally taken as a section of constant phase of the driving, the maximal control frequency is thus the driving frequency. If now the instability of the UPO is very high then the amplification of measurement noise can spoil the feedback control when controlling only once per driving period. Therefore, for experiments with large instabilities of the UPO quasicontinuous extensions of the original OGY control have been introduced by Reyl *et al.* [6] with the minimal expected deviation (MED) method and by Hübinger *et al.* [7,8] with the local control (LC) method. The, in principle, arbitrarily high control frequency is obtained by taking N equally spaced Poincaré sections Σ_n per period T of the driving as control stations. To achieve stability of the UPO a quasicontinuous OGY control thus has to work with the linearizations of the mapping $\mathbf{P}^{(n,n+1)} = \boldsymbol{\phi}|_{\Sigma_n}^{\Delta t}$, $\Delta t = T/N$, which maps a state from the Poincaré section Σ_n to the next section Σ_{n+1}. Now in the original OGY method the control requirement is based on the eigendirections of the linearized Poincaré mapping. For the quasicontinuous control methods the control requirement has to be changed as the eigenvalues of the linearized mapping $\mathbf{P}^{(n,n+1)}$ can have complex eigenvalues. Therefore the MED and LC methods use control requirements that are suited for complex eigenvalues too.

The second modification that we address comes in when one uses time delay coordinates [9–11] for the reconstruction of the attractor. In this case the OGY feedback formula has to be modified in the way that also preceding values of the control parameter have to be considered to obtain the actual value of the control parameter [12]. The reason for this modification is that for delay coordinates the Poincaré mapping depends not only on the actual control parameter, but also on all preceding ones that were changed during the time window $\tau_w = (d-1)\tau$ of the delay vector $(x(t), x(t-\tau), \dots, x(t-(d-1)\tau))$. For a quasicontinuous

control with a control frequency being, e.g., the sampling frequency $1/\Delta t$, the mapping $\mathbf{P}^{(n,n+1)} = \boldsymbol{\phi}^{\Delta t}_{|\Sigma_n}$ will depend on the last $w = l(d-1)$ parameter changes with l being the time delay in units of the sampling time and d the embedding dimension. We express this dependence as $\mathbf{z}^{n+1} = \mathbf{P}^{(n,n+1)}(\mathbf{z}^n, p^{n-w}, \ldots, p^{n-1}, p^n)$. Thus, to stabilize an UPO by a quasicontinuous OGY control using time-delay coordinates the fundamental equation of the control problem is given by the linearization of $\mathbf{P}^{(n,n+1)}$ having the form

$$\delta\mathbf{z}^{n+1} = A^n \cdot \delta\mathbf{z}^n + \sum_{i=0}^{w} \mathbf{b}^{n,i} \delta p^{n-i}, \qquad (1)$$

with $\delta\mathbf{z}^n = \mathbf{z}^n - \mathbf{z}^n_F$, $\mathbf{z}^n_F$ being the UPO in section Σ_n, and the linearizations $A^n = D_{\mathbf{z}^n}\mathbf{P}^{(n,n+1)}$ and $\mathbf{b}^{n,i} = (\partial/\partial p^{n-i})\mathbf{P}^{(n,n+1)}$ around $(\mathbf{z}_F, p_0, \ldots, p_0)$. Now, to obtain a control formula one could use the extended state vector $\mathbf{y}^n = (\mathbf{z}^n, p^{n-w}, \ldots, p^{n-1})$ and rewrite the dynamics as

$$\delta\mathbf{y}^{n+1} = C^n \cdot \delta\mathbf{y}^n + \mathbf{d}^n \delta p^n$$

with

$$C^n = \begin{pmatrix} A^n & \mathbf{b}^{n,w} & \mathbf{b}^{n,w-1} & \cdots & \mathbf{b}^{n,1} \\ & 0 & 1 & \cdots & 0 \\ \mathbf{0} & \vdots & \ddots & \ddots & \vdots \\ & \vdots & \cdots & \ddots & 1 \\ & 0 & \cdots & \cdots & 0 \end{pmatrix}$$

and $\mathbf{d}^n = (\mathbf{b}^{n,0}, 0, \ldots, 0, 1)^\dagger$. For the OGY control with time delay this was proposed by Romeiras *et al.* [13] together with a pole placement technique and later on worked out and realized in numerical experiments by So and Ott [14]. In [15] Ding *et al.* report successful control of a magnetoelastic beam experiment using time-delay coordinates and an extended state space approach. In addition to the use of the extended state space for time-delay coordinates, the work in [13–15] also generalizes the OGY control requirement in the way that also systems with more than one unstable eigendirections can be controlled with a single control parameter.

The attractiveness of the extended state space approach is that at first glance one can use the same control requirement as for the physical state space without a formal change. For the OGY approach using eigenvalues and eigendirections of the UPO as done in [13–15], this also works in practice as the eigenvalues and eigendirections in the delay space and the extended space are related in a very simple manner [14,15]. However, for the quasicontinuous control methods considered in this paper, i.e., MED or LC, it turns out that the use of the extended state space formulation leads to a scaling dependence on the units of the control parameter. Therefore, for our case we prefer another possibility to derive a control formula. We require stabilization not for $\mathbf{z}^{n+1}$ but only for $\mathbf{z}^{n+w+1}$ with $\delta p^n \neq 0$ and $\delta p^{n+1} = \cdots = \delta p^{n+w} = 0$. This control requirement coincides with the second modification of the original OGY method in [12] given for time-delay coordinates. While for the original OGY method these two approaches, i.e., the extended state space and the modified control requirement, are

equivalent, this is no longer the case for the quasicontinuous control approach. In our investigations we discuss this point.

Finally, we compare the performance of these two quasicontinuous control approaches in a bronze ribbon experiment. To test the control methods, all control vectors needed for control are extracted from the analysis of a scalar measurement signal. Furthermore, we extend the adaptive orbit correction [16] of Doerner *et al.* to time delay coordinates to correct the position of the UPO used in the feedback formula during control. In the experiment the modified control requirement will show the best result, while the extended state space approach is not suitable for the control methods discussed in this paper.

Before we start we want to mention that the control experiment presented in this paper is not the first realization of a quasicontinuous control using time-delay coordinates. Reyl *et al.* apply the MED method in a NMR-laser experiment using time-delay coordinates [6]. However, they do not consider the dependence on preceding values of the control parameter. de Korte *et al.* use the local control method and time delay coordinates to control an experimental driven pendulum [17]. In their experiment they only consider the dependence of one preceding parameter value as they use only four control stations per period of the driving and a time delay window $(d-1)\tau$, which is smaller than $T/4$. Furthermore, in their control experiment they apply the original control requirement of the local control, i.e., stabilization in the next Poincaré section, without modifying the control requirement as we do.

Our paper is now organized as follows. In Sec. II we justify theoretically the fundamental equation (1) for the linearized dynamics in time delay embedding space when quasicontinuous control is applied. In Sec. III we first briefly recall the quasicontinuous OGY control in a physical state space. Then we give the two possible extensions for time-delay embedding, i.e., the extended state space approach and the modified control requirement. After describing the bronze ribbon experiment in Sec. IV, we report, in Sec. V, our control experiments using quasicontinuous control in embedding space. Our results are summarized in Sec. VI. In Appendix A an explicit relation between the linearizations in the physical state space and the corresponding ones in the embedding space is given. In Appendix B we discuss how the linearizations in the embedding space are obtained from experimental data and how to avoid errors that are due to using for the fits nearest-neighbor points with finite distances to the UPO for which the curvature of the attractor in the embedding space can no longer be neglected.

II. LOCAL DYNAMICS IN THE TIME-DELAY EMBEDDING

In this section we want to give some theoretical underpinning to the fundamental equation (1) for quasicontinuous control with time delay coordinates that results from the dependence of the flow mapping $\mathbf{P}^{(n,n+1)} = \boldsymbol{\phi}^{\Delta t}_{|\Sigma_n}$ on the control parameter. To start with our argumentation let us denote with $\hat{\Sigma}_n$ the $N = T/\Delta t$ Poincaré sections of constant phase of the driving in the physical state space. Let $p^n = p_0 + \delta p^n$ be the value of the control parameter p when the system goes from section $\hat{\Sigma}_n$ to $\hat{\Sigma}_{n+1}$. Thus the flow mapping $\hat{\mathbf{P}}^{(n,n+1)}$ in

the physical state space that maps a state $\hat{\mathbf{z}}^n$ in $\hat{\Sigma}_n$ to a state $\hat{\mathbf{z}}^{n+1}$ in $\hat{\Sigma}_{n+1}$ can be expressed as

$$\hat{\mathbf{z}}^{n+1} = \hat{\mathbf{P}}^{(n,n+1)}(\hat{\mathbf{z}}^n, p^n)$$

or, more generally, the mapping $\hat{\mathbf{P}}^{(n,n+k)}$ from $\hat{\Sigma}_n$ to $\hat{\Sigma}_{n+k}$ has to be written as

$$\hat{\mathbf{z}}^{n+k} = \hat{\mathbf{P}}^{(n,n+k)}(\hat{\mathbf{z}}^n, p^n, p^{n+1}, \ldots, p^{n+k-1}).$$

Note that we always use a caret for the quantities referring to the dynamics in the physical state space in order to distinguish them from the corresponding ones in the time delay embedding space.

Now, for the reconstruction of the attractor we want to use time delay coordinates. For a driven system it is appropriate to retain as additional coordinate in the embedding space the phase of the driving. Doing so we can introduce N successive Poincaré sections Σ_n, $n = 1, \ldots, N$ in the embedding space that exactly correspond to the sections $\hat{\Sigma}_n$ in the orginal state space. For an embedding dimension of $d+1$ a point $\mathbf{z}^n \in \Sigma_n$ is then given by $\mathbf{z}^n = (x^n, x^{n-l}, \ldots, x^{n-(d-1)l})^\dagger$, where $x^n = x(t_0 + n\Delta t)$ is an accessible measurement signal and $\tau = l\Delta t$ an appropriately chosen time delay. This measurement process can be mathematically expressed as a scalar function h on the physical state space, i.e., $x^n = h(\hat{\mathbf{z}}^n)$. For shortness of our formulas, we assume here that the measurement does not depend on the phase of the driving. According to Takens's theorem [10,11], for an appropriately chosen time delay τ and a sufficiently high dimension d there exists a smooth, invertible embedding function Φ_n, i.e., $\mathbf{z}^n = \Phi_n(\hat{\mathbf{z}}^n)$, which maps points $\hat{\mathbf{z}}^n$ from the Poincaré section $\hat{\Sigma}_n$ to points $\mathbf{z}^n$ in the time-delay Poincaré section Σ_n. This function, which is given by $\mathbf{z}^n = \Phi_n(\hat{\mathbf{z}}^n)$ $= (h(\hat{\mathbf{z}}^n), h(\hat{\mathbf{z}}^{n-l}), \ldots, h(\hat{\mathbf{z}}^{n-(d-1)l}))^\dagger$, is closely related to the dynamics of the system and thus dependent on preceding parameter values when the control is applied. To write the states $\hat{\mathbf{z}}^{n-jl}$, $j = 1, \ldots, (d-1)$, as a function of $\hat{\mathbf{z}}^n$ the inverse $\hat{\mathbf{P}}^{(n-jl,n)-1}$ of the mapping $\hat{\mathbf{P}}^{(n-jl,n)}$ has to be used. Taking into account that $\hat{\mathbf{P}}^{(n-jl,n)}$ depends on the parameter values $p^{n-jl}, \ldots, p^{n-1}$, the embedding function Φ_n can be written as a function of $\hat{\mathbf{z}}^n$ as

$$\mathbf{z}^n = \begin{pmatrix} h(\hat{\mathbf{z}}^n) \\ h(\hat{\mathbf{P}}^{(n-l,n)-1}(\hat{\mathbf{z}}^n, p^{n-l}, \ldots, p^{n-1})) \\ h(\hat{\mathbf{P}}^{(n-2l,n)-1}(\hat{\mathbf{z}}^n, p^{n-2l}, \ldots, p^{n-1})) \\ \vdots \\ h(\hat{\mathbf{P}}^{(n-w,n)-1}(\hat{\mathbf{z}}^n, p^{n-w}, \ldots, p^{n-1})) \end{pmatrix} \quad (2a)$$

$$= \Phi_n(\hat{\mathbf{z}}^n, p^{n-w}, \ldots, p^{n-1}). \quad (2b)$$

Thus, for quasicontinuous control the embedding function Φ_n depends not only on $\hat{\mathbf{z}}^n$, but also on the last $w = (d-1)l$ parameters. For an abbreviation we write

$\mathbf{z}^n = \Phi_n(\hat{\mathbf{z}}^n, \mathbf{p}^{n-1})$, with $\mathbf{p}^{n-1} = (p^{n-w}, \ldots, p^{n-1})$, and for the unperturbed dynamics $\mathbf{z}^n = \Phi_n(\hat{\mathbf{z}}^n, \mathbf{p}_0)$, with $\mathbf{p}_0 = (p_0, \ldots, p_0) \in \mathbb{R}^w$.

This dependence of Φ_n on the preceding control parameters has direct impact on the flow mapping $\mathbf{P}^{(n,n+1)}$ in the time delay embedding space that maps $\mathbf{z}^n$ to $\mathbf{z}^{n+1}$. Starting with $\mathbf{z}^{n+1} = \Phi_{n+1}(\hat{\mathbf{z}}^{n+1}, \mathbf{p}^n)$, $\hat{\mathbf{z}}^{n+1} = \hat{\mathbf{P}}^{(n,n+1)}(\hat{\mathbf{z}}^n, p^n)$, and $\hat{\mathbf{z}}^n = \Phi_n^{-1}(\mathbf{z}^n, \mathbf{p}^{n-1})$ one can express $\mathbf{z}_{n+1}$ as a function of $\mathbf{z}_n$ as

$$\mathbf{z}^{n+1} = \Phi_{n+1}(\hat{\mathbf{P}}^{(n,n+1)}(\Phi_n^{-1}(\mathbf{z}^n, \mathbf{p}^{n-1}), p^n), \mathbf{p}^n). \quad (3)$$

But this is the flow mapping $\mathbf{P}^{(n,n+1)}$, which, as a consequence, depends on the $w = (d-1)l$ preceding values of the control parameter and the actual value p^n, i.e., we can write

$$\mathbf{z}^{n+1} = \mathbf{P}^{(n,n+1)}(\mathbf{z}^n, \mathbf{p}^{n-1}, p^n). \quad (4)$$

This finally leads directly to the fundamental equation for a quasicontinuous OGY control for time delay coordinates, which is the linearization of $\mathbf{P}^{(n,n+1)}$ around the UPO $\mathbf{z}_F^n$ and the control parameter $\mathbf{p}_0$

$$\delta\mathbf{z}^{n+1} = A^n \cdot \delta\mathbf{z}^n + \sum_{i=0}^{w} \mathbf{b}^{n,i} \delta p^{n-i},$$

with $\delta\mathbf{z}^n = \mathbf{z}^n - \mathbf{z}_F^n$, $A^n = D_{\mathbf{z}^n}\mathbf{P}^{(n,n+1)}(\mathbf{z}_F^n, p_0, \ldots, p_0)$, and $\mathbf{b}^{n,i} = (\partial/\partial p^{n-i})\mathbf{P}^{(n,n+1)}(\mathbf{z}_F^n, p_0, \ldots, p_0)$.

In Appendix A we support this result by giving an explicit relation between the linearizations $\hat{A}^n = D_{\hat{\mathbf{z}}^n}\hat{\mathbf{P}}^{(n,n+1)}$ and $\hat{\mathbf{b}}^n = (\partial/\partial p^n)\hat{\mathbf{P}}^{(n,n+1)}$ in the physical state space and the linearizations A^n and $\mathbf{b}^{n,i}$ in the time-delay embedding space. In Appendix B we confirm this relation further in a numerical experiment of a Duffing oscillator with a known measurement function h. In addition, we describe the pitfalls that have to be avoided when determining A^n and $\mathbf{b}^{n,i}$ from nearest neighbors whose finite distances to the UPO already experience the curvature of the attractor in the embedding space. As a remedy we propose the projection to the corresponding tangent spaces. In the simulation of the Duffing oscillator we demonstrate that this projection helps to improve the determination of A^n and $\mathbf{b}^{n,i}$ considerably.

III. QUASICONTINUOUS CONTROL USING TIME-DELAY COORDINATES

In this section we first briefly recall the quasicontinuous control in a physcial state space. We give a unified formulation for the local control method and the minimal expected deviation method. Both methods are slightly changed compared to their first publication. After the presentation of the explicit feedback formulas we describe two different ways to obtain control formulas when a time delay embedding is used. These are the extended state space approach and a modification of the control requirement. In fact, for the OGY control method both possibilities have been studied. In [13–15] the extended state space approach is used for delay vectors in combination with an extension of the OGY method for more than one unstable direction. In [12,18] the modified control requirement is given for the original OGY method.

While for the original OGY method with one unstable eigen-direction both approaches yield the same control formula, for the quasicontinuous control methods considered here the resulting control formulas differ substantially, as we will show.

A. Quasicontinuous control in physical state space

Quasicontinuous control for a driven system refers to the adjustment of the control parameter every $\Delta t = T/N$ whenever the trajectory intersects one of the N equally spaced Poincaré sections. As in Sec. II, we denote with $\hat{\mathbf{P}}^{(n,n+1)}$ the flow mapping in the physical state space that maps a state $\hat{\mathbf{z}}^n$ to a state $\hat{\mathbf{z}}^{n+1}$. The starting point of a quasicontinuous OGY control is the linearization of $\hat{\mathbf{P}}^{(n,n+1)}$ around the UPO $\hat{\mathbf{z}}_F^n$ and p_0,

$$\delta\hat{\mathbf{z}}^{n+1} = \hat{A}^n \cdot \delta\hat{\mathbf{z}}^n + \hat{\mathbf{b}}^n \delta p^n, \tag{5}$$

with

$$\hat{A}^n = D_{\hat{\mathbf{z}}^n}\hat{\mathbf{P}}^{(n,n+1)}(\hat{\mathbf{z}}_F^n, p_0)$$

and

$$\hat{\mathbf{b}}^n = (\partial/\partial p^n)\hat{\mathbf{P}}^{(n,n+1)}(\hat{\mathbf{z}}_F^n, p_0).$$

Now, already in two dimensions the linearization $\hat{A}^n$ of the mapping $\hat{\mathbf{P}}^n$ can have complex eigenvalues. Therefore, the OGY control condition that the next state $\hat{\mathbf{z}}^{n+1}$ falls on the stable eigendirection of $\hat{A}^n$, which is formalized as $\hat{\mathbf{f}}_u^n \cdot \delta\hat{\mathbf{z}}^{n+1} = 0$, with $\hat{\mathbf{f}}_u^n$ being the contravariant unstable eigenvector, cannot be used anymore. The LC method and the MED method solve this problem by posing a control requirement that does not depend on the eigendirections of $\hat{A}^n$.

In the local control method Hübinger *et al.* use the singular value decomposition (SVD) of $\hat{A}^n$ in order to formulate a control condition. Let $\hat{A}^n = \hat{U}^n \cdot \hat{W}^n \cdot \hat{V}^{n\dagger}$ denote the singular value decomposition of $\hat{A}^n$ with the orthogonal matrices $\hat{U}^n$ and $\hat{V}^n$ having as column vectors $\hat{\mathbf{u}}_i^n$ and $\hat{\mathbf{v}}_i^n$ and the diagonal matrix $\hat{W}^n$ with positive entries $\hat{w}_i^n$, the singular values. Having calculated the SVD, the action of $\hat{A}^n$ can be described as $\hat{A}^n \cdot \hat{\mathbf{v}}_i^n = \hat{w}_i^n \hat{\mathbf{u}}_i^n$. Thus the orthonormal basis $\{\hat{\mathbf{v}}_i^n\}$ is mapped on the orthonormal basis $\{\hat{\mathbf{u}}_i^n\}$ with an additional stretching or shrinking by the singular values $\hat{w}_i^n$. Having the singular values ordered by size $\hat{\mathbf{v}}_1^n$ is the unstable direction of $\hat{A}^n$ (here we assume that only one unstable direction exists). In the local control method one requires that the projection of $\delta\hat{\mathbf{z}}^{n+1}$ on the unstable direction $\hat{\mathbf{v}}_1^{n+1}$ is diminished. Thus, for perfect stabilization the control requirement of the local control could be written as

$$\hat{\mathbf{v}}_1^{n+1\dagger} \cdot \delta\hat{\mathbf{z}}^{n+1} = 0. \tag{6}$$

In the minimal expected deviation method Reyl *et al.* use another control requirement. They require that the distance $\|\delta\hat{\mathbf{z}}^{n+1}\|$ to the UPO in $\hat{\Sigma}_{n+1}$ is minimized. In order to find this minimum the derivative of $\|\delta\hat{\mathbf{z}}^{n+1}\|^2$ with respect to

δp^n is calculated and its zeros have to be determined. This calculation leads to the condition

$$\hat{\mathbf{b}}^{n\dagger} \cdot \delta\hat{\mathbf{z}}^{n+1} = 0. \tag{7}$$

Thus, also the control requirement of MED can be expressed in the way that the projection of $\delta\hat{\mathbf{z}}^{n+1}$ on a special direction vanishes. If one compares Eqs. (6) and (7) the control requirement of the LC method and the MED method differs only with respect to the special choice of this direction.

To proceed with the derivation of an explicit control formula let us call this direction for a moment $\hat{\mathbf{h}}^n$. As was said, the most pretentious control requirement would be $\hat{\mathbf{h}}^{n\dagger} \cdot \delta\hat{\mathbf{z}}^{n+1} = 0$. In the paper of Reyl *et al.* this maximal control requirement is used for $N = 4$ control stations per period. But if the number N of the control stations increases the time of the control action $\Delta t = T/N$ decreases. If the maximal control requirement were retained the small control time Δt would lead to a large control signal δp^n. In order to avoid large control signals for high control frequencies Hübinger *et al.* propose to weaken the control requirement. In the LC method they introduce a decay factor $1-\rho$ in the control requirement [7]. We follow this idea, but formulate the reduced control condition in a slightly different way, which leads to better control results. We require that the application of the control signal δp^n diminishes the projection of $\delta\hat{\mathbf{z}}^{n+1}$ on $\hat{\mathbf{h}}^n$ by a factor $1-\rho$ compared to the one that $\delta\hat{\mathbf{z}}^{n+1}_{\delta p^n=0}$ would have if no control were applied, i.e.,

$$\hat{\mathbf{h}}^{n\dagger} \cdot \delta\hat{\mathbf{z}}^{n+1} = (1-\rho)\hat{\mathbf{h}}^{n\dagger} \cdot \delta\hat{\mathbf{z}}^{n+1}_{\delta p^n=0}. \tag{8}$$

Inserting Eq. (5) into Eq. (8) gives the explicit control formula for the quasicontinuous control

$$\delta p^n = -\rho \frac{\hat{\mathbf{h}}^{n\dagger} \cdot \hat{A}^n}{\hat{\mathbf{h}}^{n\dagger} \cdot \hat{\mathbf{b}}^n} \cdot \delta\hat{\mathbf{z}}^n, \tag{9}$$

with $\hat{\mathbf{h}}^n = \hat{\mathbf{v}}_1^{n+1}$ for the LC method and $\hat{\mathbf{h}}^n = \hat{\mathbf{b}}^n$ for the MED method. With Eq. (9) we have the general feedback formula for quasicontinuous control in physcial state space if the linearization of $\hat{\mathbf{P}}^{(n,n+1)}$ are given by Eq. (5).

B. Control formula using extended states

Now we proceed with the quasicontinuous control in the time delay embedding space when the starting point of the derivation of the feedback formula is the linearization

$$\delta\mathbf{z}^{n+1} = A^n \cdot \delta\mathbf{z}^n + \sum_{i=0}^{w} \mathbf{b}^{n,i} \delta p^{n-i}.$$

We start with the extended state space approach [13–15]. An extended state is given by $\mathbf{y}^n = (\mathbf{z}^n, \mathbf{p}^{n-1})^\dagger$. Thus with the extended states the preceding parameter dependences $\mathbf{p}^{n-1} = (p^{n-w}, \ldots, p^{n-1})$ are considered as state variables. Doing so, the linearized dynamics (1) can be written as

$$\delta\mathbf{y}^{n+1} = C^n \cdot \delta\mathbf{y}^n + \mathbf{d}^n \delta p^n, \tag{10}$$

with

$$C^n = \begin{pmatrix} A^n & \mathbf{b}^{n,w} & \mathbf{b}^{n,w-1} & \cdots & \mathbf{b}^{n,1} \\ \mathbf{0} & & N_w & & \end{pmatrix}, \qquad (11a)$$

the $w \times w$ nilpotent block N_w

$$N_w = \begin{pmatrix} 0 & 1 & \cdots & 0 \\ \vdots & \ddots & \ddots & \vdots \\ \vdots & \cdots & \ddots & 1 \\ 0 & \cdots & \cdots & 0 \end{pmatrix} \qquad (11b)$$

and

$$\mathbf{d}^n = (\mathbf{b}^{n,0}, 0, \ldots, 0, 1)^\dagger. \qquad (11c)$$

Note that Eq. (10) has the same form as the linear approximation (5) in the physical state space. Therefore, the control requirement can be chosen in complete analogy to Eq. (8). This leads to the control formula

$$\delta p^n = -\rho \frac{\mathbf{h}^{n\dagger} \cdot C^n}{\mathbf{h}^{n\dagger} \cdot \mathbf{d}^n} \cdot \delta \mathbf{y}^n, \qquad (12)$$

with $\mathbf{h}^n = \mathbf{v}_1^{n+1}$ the singular vector corresponding to the largest singular value of C^{n+1} for the LC method and $\mathbf{h}^n = \mathbf{d}^n$ for the MED method. For the local control method we assume that the largest singular value w_1^{n+1} of C^{n+1} is the only singular value that is larger than 1.

From a formal point of view, the problem of quasicontinuous control with time delay coordinates could be regarded as solved. But, as was already mentioned in the Introduction, the at first glance simple and convincing use of the extended states leads, for the quasicontinuous control methods considered here, to an undesirable dependence on the units of the control parameter p. We demonstrate this by showing that the control formula (12) depends on the scaling of the parameter p. To do this we replace all parameters p^n by p^n/σ and all vectors $\mathbf{b}^{n,i}$ by $\sigma \mathbf{b}^{n,i}$. Taking the structure of $\mathbf{y}^n = (\mathbf{z}^n, p^{n-1})^\dagger$ and C^n, $\mathbf{d}^n$ in Eq. (11) into account, we obtain in the case of the MED method ($\mathbf{h}^n = \mathbf{d}^n$) the following expression for Eq. (12):

$$\delta p^n = -\rho \frac{\mathbf{b}^{n,0\dagger} \cdot \left[A^n \cdot \delta \mathbf{z}^n + \sum_{i=1}^{w} \mathbf{b}^{n,i} \delta p^{n-i} \right]}{\mathbf{b}^{n,0\dagger} \cdot \mathbf{b}^{n,0} + \sigma^{-2}}. \qquad (13)$$

Due to the appearance of σ^{-2} in the denominator, this control formula is not invariant with respect to the scaling factor σ. A similar result is obtained for the LC method in which the scaling dependence is caused by the singular value decomposition of C^n. The deeper reason for this is that, although the equation (10) for the linearized dynamics in the extended state space is invariant under a scaling of the control parameter, the control requirements [Eqs. (6), (7), or (8)] of the LC and MED methods are not invariant under a rescaling of p if they are formulated in the extended state space. For the MED method this can directly be seen inserting $\mathbf{d}^n$ and $\delta \mathbf{y}^{n+1}$ in the control requirement (7) or (8). For the LC method one has to have in mind that the control requirement (6) is based on the SVD of C^{n+1}. But a rescaling of p can be

viewed as a coordinate transformation and, as is well known, the SVD is not invariant under a coordinate transformation. Thus, for both quasicontinuous methods the use of an extended state space shows an undesirable dependence on the units of the control parameter. The control experiments in Sec. V will show that this dependence indeed causes a breakdown of the control for certain choices of the scaling parameter σ. In contrast to this, the extended state approach in [13–15] is combined with a control requirement based upon eigenvalues of the controlled problem [13] or the eigendirections of the UPO [14,15]. As the eigenvalues are invariant under a transformation of coordinates, no problem arises with the pole placement technique in [13]. The use of the eigendirections of the UPO in [14,15] for the control requirement does not lead to the above-discussed problem either. This is so because the eigendirections of the linearized Poincaré mapping A and the associated matrix C in the extended state space obey a very simple relationship [14,15] that is preserved under a coordinate transformation. If we denote with $\mathbf{e}_i^u$ and $\mathbf{e}_i^s$ the unstable and stable eigendirections of the $d \times d$ matrix A, then the unstable eigendirections of the $(d+w) \times (d+w)$ matrix C are given by $(\mathbf{e}_i^u, 0, \ldots, 0)^\dagger \in \mathbb{R}^{d+w}$ and the stable directions by $(\mathbf{e}_i^s, 0, \ldots, 0)^\dagger \in \mathbb{R}^{d+w}$ and an arbitrarily chosen w-dimensional basis of the null space of C^w [15]. This relationship between the eigendirections of A and C is not affected by a change of scales of the control parameter p. Therefore, the use of the extended state space works fine for the control requirements used in [13–15].

C. The modified control requirement

An alternative way to derive a feedback formula starting from the linearization (1) is to modify the control requirement. For the original OGY method with time delay coordiantes this was done in [12,18] for the special case that only one preceding parameter dependence appears in the linearization. The control requirement was modified in the way that the system had to stabilize only in two control steps, i.e., for $\mathbf{z}^{n+2}$, for an appropriately chosen parameter perturbation $\delta p^n \neq 0$ and $\delta p^{n+1} = 0$. We generalize this modified control requirement for general w and the linearization (1) of the quasicontinuous control. Because the parameter value p^n influences the trajectory $\mathbf{z}^{n+1}, \mathbf{z}^{n+2}, \ldots$ until $\mathbf{z}^{n+w}$, we require that the system stabilizes only after $w+1$ time steps for an appropriately chosen parameter perturbation $\delta p^n \neq 0$ without further control interventions in between, i.e., the modified control requirement is

$$\mathbf{h}_w^{n\dagger} \cdot \delta \mathbf{z}^{n+w+1} = (1-\rho) \mathbf{h}_w^{n\dagger} \cdot \delta \mathbf{z}_{\delta p^n = 0}^{n+w+1}, \qquad (14a)$$

$$\delta p^{n+1} = \delta p^{n+2} = \cdots = \delta p^{n+w} = 0. \qquad (14b)$$

The condition (C14a) is chosen in complete analogy to Eq. (8) with $\delta \mathbf{z}_{\delta p^n = 0}^{n+w+1}$ denoting the distance vector to $\mathbf{z}_F^{n+w+1}$, which $\mathbf{z}^{n+w+1}$ would have if no control at all (i.e., $\delta p^n = 0$) were used. The direction $\mathbf{h}_w^n$ depends on w and is chosen below in such a way that the LC method and the MED method are obtained.

To derive an explicit control formula, $\delta \mathbf{z}^{n+w+1}$ and $\delta \mathbf{z}_{\delta p^n = 0}^{n+w+1}$ in Eq. (14a) have to be expressed as a

function of the actual state $\delta \mathbf{z}^n$. This is done by using the linearizations $A_w^n = D_{\mathbf{z}^n} \mathbf{P}^{(n,n+w+1)}(\mathbf{z}_F^n, p_0, \ldots, p_0)$ and $\mathbf{b}_w^{n,i} = (\partial/\partial p^{n-i}) \mathbf{P}^{(n,n+w+1)}(\mathbf{z}_F^n, p_0, \ldots, p_0)$ and taking the condition (14b) into account. One obtains

$$\delta \mathbf{z}^{n+w+1} = A_w^n \cdot \delta \mathbf{z}^n + \sum_{i=0}^{w} \mathbf{b}_w^{n,i} \delta p^{n-i}. \quad (15)$$

The matrices A_w^n are given by $A_w^n = A^{n+w} \cdots A^n$. The vectors $\mathbf{b}_w^{n,i}$ can be recursively calculated using $\mathbf{b}_0^{n,i} = \mathbf{b}^{n,i}$ and

$$\mathbf{b}_j^{n,i} = \begin{cases} A^{n+j} \cdot \mathbf{b}_{j-1}^{n,i} & \text{for } j > i \\ A^{n+j} \cdot \mathbf{b}_{j-1}^{n,i} + \mathbf{b}^{n+j,i-j} & \text{for } j \leq i. \end{cases}$$

Inserting Eq. (15) in Eq. (14a) yields the desired control formula

$$\delta p^n = -\rho \frac{\mathbf{h}_w^{n\dagger} \cdot \left[A_w^n \cdot \delta \mathbf{z}^n + \sum_{i=1}^{w} \mathbf{b}_w^{n,i} \delta p^{n-i} \right]}{\mathbf{h}_w^{n\dagger} \cdot \mathbf{b}_w^{n,0}}. \quad (16)$$

For the LC method, the direction $\mathbf{h}_w^n$ is given by $\mathbf{h}_w^n = \mathbf{v}_1^{n+w+1}$, where $\mathbf{v}_1^{n+w+1}$ is the singular vector of A^{n+w+1}, which refers to the direction of maximal stretching. For the MED method the direction has to be chosen as $\mathbf{h}_w^n = \mathbf{b}_w^{n,0}$ in order to minimize the deviation of the trajectory from the desired orbit in section Σ_{n+w+1}. Both possible directions lead to a control formula that does not depend on a scaling factor of the control parameter, in contrast to the control formula (12) using extended states. The simple reason for this is that not only the linearized dynamics (1), but also the control requirement (14a) with Eq. (15) is not affected by a rescaling of p.

Note that in the formulation of the modified control requirement ($\delta p^{n+1} \neq 0$ and $\delta p^{n+1} = \cdots = \delta p^{n+w} = 0$) and the consecutive derivation of the control formula (16), the parameter perturbations are in principle calculated until δp^{n+w}. In the experimental realization, however, where noise is always present, we calculate δp^n at every control step n once again in order to use the possibility to correct the parameter perturbation using the actual measurements of the system.

Now we want to test the performance of the two different control formulas (12) and (16) in a mechanical experiment. For the control experiments all control vectors needed for the control formulas are extracted from the analysis of a scalar measurement signal. Before the results of these control experiments are reported we first describe the experimental setup.

IV. THE BRONZE RIBBON EXPERIMENT

A. Experimental setup

The experiment was stimulated by the magnetoelastic beam experiment of Moon [19]. A detailed description can be found in [8]. The experiment is a horizontally cantilevered elastic bronze ribbon equipped with two small permanent magnets (see Fig. 1). The beam is located in an inhomogeneous magnetic field. To drive the system two coils are
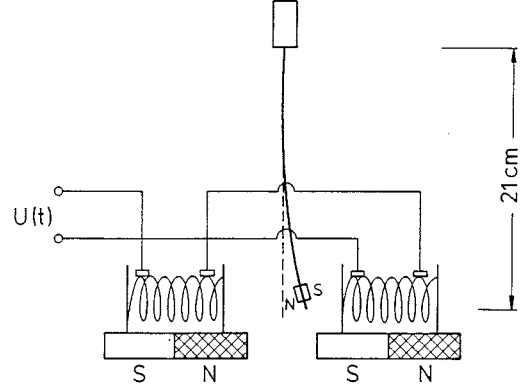

FIG. 1. Experimental setup of the chaotic bronze ribbon. A horizontally cantilevered bronze beam equipped with two small permanent magnets is located in an inhomogeneous magnetic field. Two coils are placed around the free end of the beam and are supplied with an ac voltage $U(t) = U_A \sin \omega t + p$, with $U_A = 0.6$ V and $T = 2\pi/\omega = 1$ s. The offset voltage p is used as control parameter. Measurements are taken with a wire strain gauge at the fixed end of the beam to obtain a voltage signal x related to the deflection of the beam.

placed around the free end of the beam and supplied with an ac voltage $U(t) = U_A \sin(2\pi/T)t + p$ with $U_A = 0.6$ V and the driving period $T = 1$ s. The offset voltage p is used as the control parameter, which can be adjusted via a 12-bit resolution digital-analog converter from a 486 personal computer (PC).

As the measurement signal $x(t)$ we use the voltage signal of a wire strain gauge that is related to the deflection of the vibrating beam. Using a 12-bit resolution analog-digital converter the voltage signal is transferred to the PC. Setting the sampling time Δt of the converter to $T/64$, we introduce $N = 64$ Poincaré sections for the control.

B. Determination of the control vectors

With the sampled measurement signal $x^n = x(t_0 + n\Delta t)$ the dynamics of the system is reconstructed using two time delay coordinates (x^n, x^{n-l}) and the phase of the periodic driving $U_A \sin(2\pi/T)t$. The use of two time-delay coordinates with a time lag $l = 5$ is suggested by the integral local deformation method of Buzug and Pfister [20], which we applied in order to determine optimal parameters τ and d for the time-delay embedding.

When the control parameter is set to $p_0 = -0.2$ V a chaotic attractor with correlation dimension $D_2 \approx 2.75$ in the embedding space is found (Fig. 2). Embedded in the chaotic attractor, four period-one UPOs [Figs. 3(a)–3(d)], one period-two UPO [Fig. 3(e)], and one period-three UPO [Fig. 3(f)] are detected using the method of best recurrent points described in [8]. All UPOs are also found using three time delay coordinates or using differential coordinates, i.e., $\mathbf{z}^n = (x^n, \dot{x}^n)$, to reconstruct the dynamics of the beam. For differential coordinates successful control and tracking of the UPOs are already described in [8] and [21].

The linearizations A^n of the mappings $\mathbf{P}^{(n,n+1)}$ around an UPO are extracted from the dynamics of the nearest-neighbor points in the time-delay embedding space. From
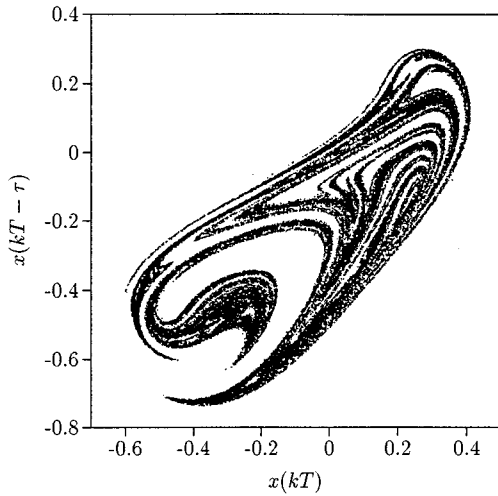
FIG. 2. Chaotic attractor for the bronze ribbon for $p_0 = -0.2$ V. 50 000 points $\mathbf{z}^n = (x^n, x^{n-l})$ are shown in the Poincaré section Σ_1 with time delay $\tau = 5\Delta t$, $\Delta t = T/64$. The correlation dimension of the attractor in the Poincaré section is calculated as $D_2 \approx 1.75$.

50 000 driving periods we extract 300 nearest-neighbor points $\mathbf{z}^n$ in each Poincaré section to fit the matrix A^n to the model $\delta \mathbf{z}^{n+1} = A^n \cdot \delta \mathbf{z}^n$. To obtain the dependences $\mathbf{b}^{n,i}$ on the control parameter we record a second time series (again 50 000 driving periods), where the control parameter is dis-
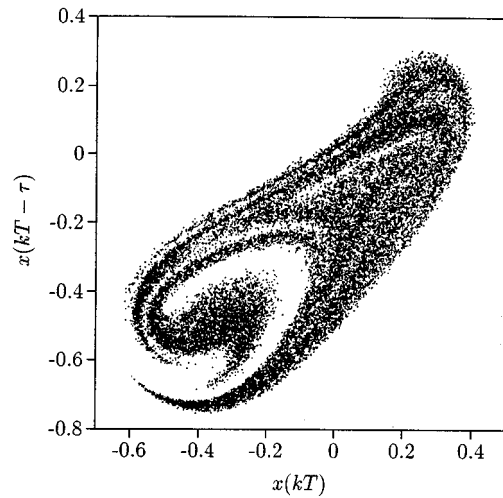

FIG. 4. Poincaré section of the chaotic attractor when the system is disturbed in each time step by a small random perturbation $\delta p^n \in [-0.07$ V, $+0.07$ V$]$. This perturbed attractor should be compared with the unperturbed attractor in Fig. 2.

turbed at each time step by a random perturbation $\delta p^n \in [-0.07$ V, $+0.07$ V$]$. These perturbations do not change significantly the global dynamics of the system as Fig. 4 compared with Fig. 2 shows. Now the vectors $\mathbf{b}^{n,i}$ are fitted to the equation $\delta \mathbf{z}^{n+1} - A^n \cdot \delta \mathbf{z}^n = \sum_{i=0}^{w} \mathbf{b}^{n,i} \delta p^{n-i}$ using the matrix A^n and 300 nearest-neighbor points. A more detailed description for the determination of the linearizations is given in Appendix B.

V. CONTROLLING THE BRONZE RIBBON

Before we discuss the control experiments to compare the performance of the quasicontinuous control for time delay coordinates based on the formulas (12) and (16) we first want to describe the adaptive orbit correction of Doerner *et al.* [16]. We always use this procedure in order to redetermine the position of the reference UPO $\mathbf{z}_F^n$ used in the feedback formula before we start with the actual control experiment in question.

A. The adaptive orbit correction

This procedure improves the control performance of every OGY-based control method considerably because it helps to deal with drifting parameters that affect the true position of an UPO. As Schwartz and Triandaf already reported for the original OGY method in [4], an errror in the determination of the UPO leads to a systematic deviation of the averaged control signal from zero. For the quasicontinuous control Doerner *et al.* observed that a difference between the true UPO $\mathbf{z}_{F,\text{true}}^n$ of the system and the orbit $\mathbf{z}_F^n$ used in the feedback control formula leads to an almost periodic trajectory $\mathbf{z}^n \approx \mathbf{z}^{n+N}$ and an almost periodic control signal $\delta p^n \approx \delta p^{n+N}$ (Fig. 5). The adaptive orbit correction enables one to calculate a new estimate of $\mathbf{z}_{F,\text{true}}^n$ during control by exploiting the periodicity of $\mathbf{z}^n$ and δp^n.

We describe the adaptive orbit correction in the context of quasicontinuous control using time-delay coordinates. The basic idea is the following. As the controlled trajectory $\mathbf{z}^n$ is
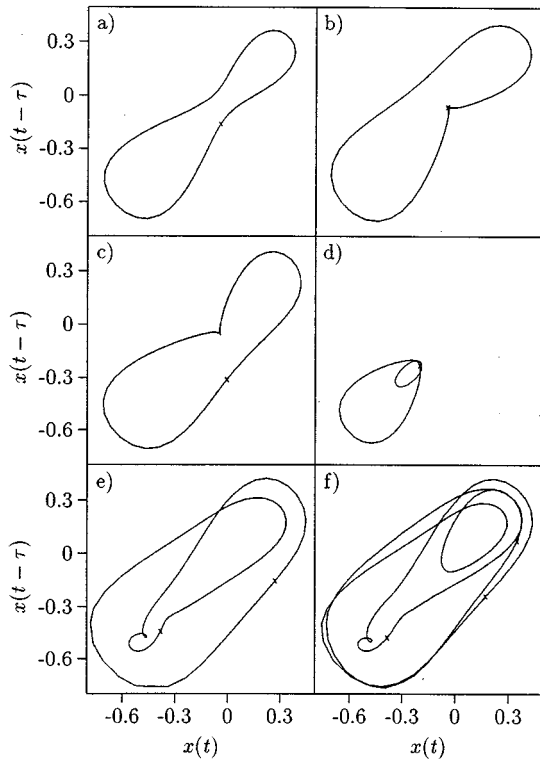

FIG. 3. Four unstable period-one orbits (a)–(d), the unstable period-two orbit (e), and the unstable period-three orbit (f) of the bronze ribbon, which have been detected by analyzing best recurrent points for $p_0 = -0.2$ V. They are shown in the $x(t)$-$x(t-\tau)$ plane with $\tau = 5\Delta t$.
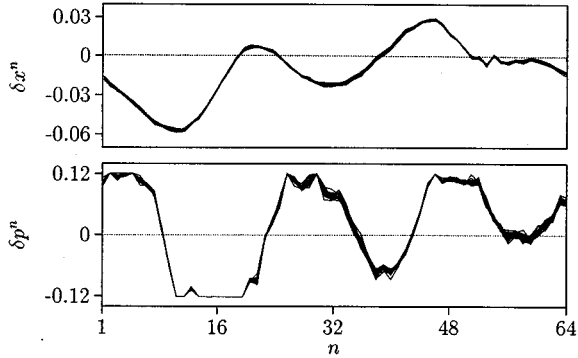
FIG. 5. Quasicontinuous control of UPO 1 using $\mathbf{z}_F^n$ extracted from the analysis of best recurrent points. Twenty periods of the controlled orbits are recorded. In the upper part the differences $\delta x^n = x^n - x_F^n$ between the desired orbit x_F^n used in the feedback control and the observed trajectory x^n and in the lower part the applied parameter perturbations δp^n for successful control are shown versus n for 20 periods of control.

still close to the true UPO $\mathbf{z}_{F,\text{true}}^n$ and the parameter perturbations δp^n are small, in each section $\Sigma_n, n = 1, \ldots, N$, $\mathbf{z}^n$ and δp^n have to fulfill the linearized dynamics

$$\mathbf{z}^{n+1} - \mathbf{z}_{F,\text{true}}^{n+1} = A^n \cdot (\mathbf{z}^n - \mathbf{z}_{F,\text{true}}^n) + \sum_{i=0}^{w} \mathbf{b}^{n,i} \delta p^{n-i}, \quad (17)$$

with $A^n = A^{n+N}$, $\mathbf{b}^{n,i} = \mathbf{b}^{n+N,i}$, and $\mathbf{z}_{F,\text{true}}^n = \mathbf{z}_{F,\text{true}}^{n+N}$. For perfect periodicity of δp^n and $\mathbf{z}^n$ this set of N vector equations can be solved with respect to $\mathbf{z}_{F,\text{true}}^n$ to obtain a new guess $\mathbf{z}_{F,\text{new}}^n$ of the true orbit $\mathbf{z}_{F,\text{true}}^n$. In the case of time-delay coordinates it is not necessary to solve the whole set of N vector equations (17). Because of the special structure of a time-delay vector $\mathbf{z}^n = (x^n, x^{n-l}, \ldots, x^{n-w})^\dagger$, already the first component of each of the N equations suffices to determine a whole time delay UPO $\mathbf{z}_{F,\text{new}}^n = (x_{F,\text{new}}^n, x_{F,\text{new}}^{n-l}, \ldots, x_{F,\text{new}}^{n-w})^\dagger$. Thus, for time-delay coordinates one solves the set of N scalar equations

$$x^{n+1} - x_{F,\text{true}}^{n+1} = \sum_{i=0}^{d-1} a_{1,i+1}^n (x^{n-il} - x_{F,\text{true}}^{n-il})$$
$$+ \sum_{i=0}^{w} b_1^{n,i} \delta p^{n-i}, \quad n = 1, \ldots, N \quad (18)$$

with respect to $x_{F,\text{true}}^n$ to obtain a new estimate $x_{F,\text{new}}^n, n = 1, \ldots, N$, to build $\mathbf{z}_{F,\text{new}}^n$. Of course, this holds only for perfect periodicity of δp^n and x^n. Because of measurement noise in experiments, one averages δp^n and x^n over some periods (in the experiment we use four periods) and inserts the averages $\langle \delta p^n \rangle$ and $\langle x^n \rangle$ instead of δp^n and x^n into the set of equations (18). Nevertheless, due to errors of A^n and $\mathbf{b}^{n,i}$ we cannot expect that the new estimate $\mathbf{z}_{F,\text{new}}^n$ gives already the correct value of $\mathbf{z}_{F,\text{true}}^n$. Therefore, we use a weighted average $\mathbf{z}_F^n(\chi) = \chi \mathbf{z}_{F,\text{new}}^n + (1-\chi) \mathbf{z}_{F,\text{old}}^n$, $\chi \in [0,1]$, in the feedback control. Starting with $\chi = 0$, we increase χ slowly until no further decrease of the control signal can be achieved. Using the orbit resulting from optimal value of χ, the next correction step is repeated. After
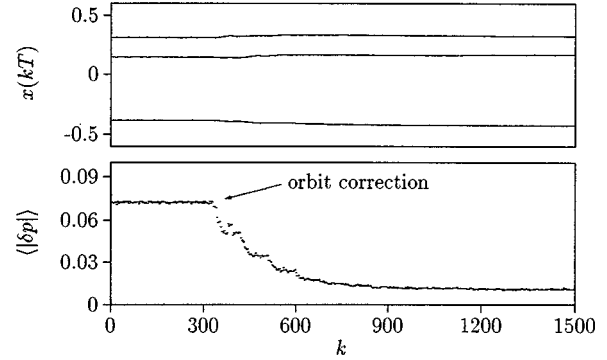

FIG. 6. Repeated orbit correction of the period-three orbit shown in Fig. 3(f) beginning with the orbits extracted from the analysis of recurrent points: In the upper part the stroboscopic measurement $x(kT)$ in the Poincaré section Σ_1 and in the lower part the averaged control signal $\langle |\delta p^n| \rangle$ over one period of the UPO are shown for 1500 periods.

some repetitions the applied averaged control signal $\langle |\delta p| \rangle$ is minimized. This procedure is shown in Fig. 6 for the period-three orbit [Fig. 3(f)]. As can be seen with this procedure, the adaptive orbit correction leads to a reduction of the averaged control signal by a factor of about 7. Depending on the initial error in the determination of the true UPO, we also observed a reduction factor 10.

B. Quasicontinuous control with time-delay coordinates

Before we report the results of our control experiments, we mention the additional control rule that we always use in our control experiments. To stabilize the UPO the control signal δp^n calculated from Eq. (12) or (16) is only applied when its magnitude is less than a maximal allowed parameter perturbation δp_{max}. In addition, control is also applied if $\|\delta \mathbf{z}^n\|$ is less than a maximal distance δz_{max}, but the calculated parameter perturbation exceeds δp_{max} [8]. In this case we only restrict the control to δp_{max} and give the control signal the sign of the calculated δp^n. This additional control rule ensures that control is never suspended if the system is close enough to the UPO.

To study the performance of the quasicontinuous control in the mechanical experiment we concentrate on the period-one orbit of Fig. 3(a), which we call UPO 1. The results do not vary significantly from the other UPOs.

First, we try to stabilize UPO 1 using the control formula (12) making use of the extended states. As was already discussed in Sec. III B for the quasicontinuous control methods (LC or MED), the control formula (12) depends on the choice of the units of the control parameters p. To investigate the effect of this dependence in the experiment we replace all parameters p^n by p^n/σ and the corresponding vectors $\mathbf{b}^{n,i}$ by $\sigma \mathbf{b}^{n,i}$ and apply the local control using (12) for different scaling factors σ. In Fig. 7 we show the experimental result for the local control method using $\sigma = 20$, $\sigma = 200$, $\sigma = 2000$, $\sigma = 20\,000$, and $\sigma = 200\,000$. As can be seen, successful control can only be achieved for $\sigma = 200$ and $\sigma = 2000$. Furthermore, the calculated control signal clearly depends on the scaling factor σ. We did the same experiment for the MED method using the extended states. As for the
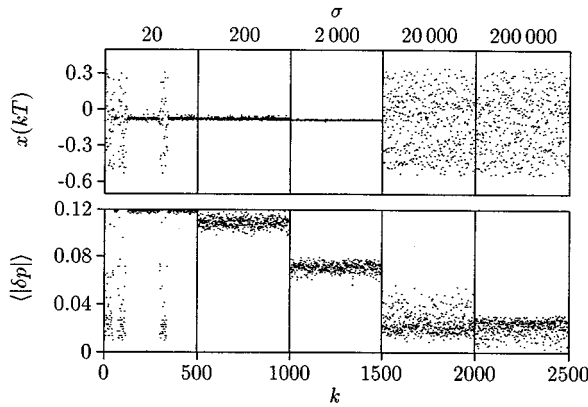
FIG. 7. Local control of UPO 1 using extended states with $\delta z_{max} = 0.1$, $\delta p_{max} = 0.12$ V, and $\rho = 0.15$. Starting with the scaling factor $\sigma = 20$, every 500 driving periods the scaling factor σ is increased by a factor 10. In the upper part the stroboscopic measurement $x(kT)$ in the Poincaré section Σ_1 and in the lower part the applied control amplitude $\langle |\delta p| \rangle$ averaged over one period of the driving are shown as functions of the period k.

LC method, only for certain values of σ, however, different from the ones for the LC experiment, could control be reached also with the MED method. There is no simple rule how to find the right values of σ. We observe that the appropriate value depends on the method and even on the parameters d, τ of the time-delay embedding. The best choice with respect to control cannot be predicted in advance. Thus using MED or LC control in the extended state space requires a blind search in the control experiment for the right units of p.

Next we want to investigate the performance of the quasicontinuous control if one uses the control formula (16) that results from the modified control requirement (14). Here one requires that the system stabilizes only after $w + 1$ time steps. For the time delay embedding with $d = 2$ and $l = 5$ the window length $w = (d-1)l$ is 5 and therefore the stabilization has to be required after six time steps. To demonstrate that the modified control requirement (14) is indeed necessary we apply local control to UPO 1 using a feedback control formula that results if one requires stabilization after $j = 1, 2, \ldots$, until nine time steps. Figure 8 shows the result of this experiment. It is clearly visible that for $j = 1$ and $j = 2$ no successful control is achieved. The UPO can be stabilized for $j \geq 3$, but the control signal is minimized for $j = 7$. A further investigation shows that the averaged distance between the UPO and the trajectory of the system has a minimum for $j = 5$. Both results confirm our theoretical choice $j = w + 1$. With this choice we could stabilize all UPOs of Fig. 3 using the MED or the LC method in Eq. (16). In Fig. 9 we show an example of a successful control experiment using the LC method. Every 500 driving periods we switch from one UPO to the next one. As can be seen, the transient time to stabilize the next UPO is always very short. We did the same experiment for the MED method. There was no qualitative difference between the MED or the LC method as long as one used the modified control requirement with $j = w + 1$.

VI. SUMMARY AND CONCLUSIONS

In a bronze ribbon experiment we have implemented quasicontinuous versions of the OGY control method using
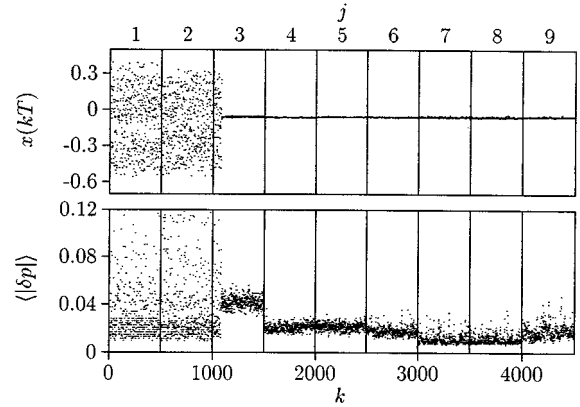

FIG. 8. Local control of UPO 1 using the modified control requirement with $\delta z_{max} = 0.1$, $\delta p_{max} = 0.12$ V, and $\rho = 0.15$. In the upper part the stroboscopic measurement $x(kT)$ in the Poincaré section Σ_1 and in the lower part the applied control amplitude $\langle |\delta p| \rangle$ averaged over one period of the driving are shown as functions of the period k. From 0 to 499 the stabilization is demanded after $j = 1$ time step; afterward the value j is increased every 500 periods by 1.

time-delay coordinates for the reconstruction of the attractor. With quasicontinuous we refer to control methods with, in principle, arbitrarily high control frequencies that are especially advantageous for highly unstable systems. In the bronze ribbon experiment we apply as quasicontinuous methods the local control method and the minimal expected deviation method. Both methods achieve a high control frequency by introducing several Poincaré sections per period of the driving. As is known for the original OGY method, for time delay coordinates the feedback law has to be modified in a way that also preceding values of the control parameter have to be included in the control formula. For a quasicontinuous control with high control frequency being, e.g., the sampling frequency $1/\Delta t$, there are $w = l(d-1)$ preceding parameter
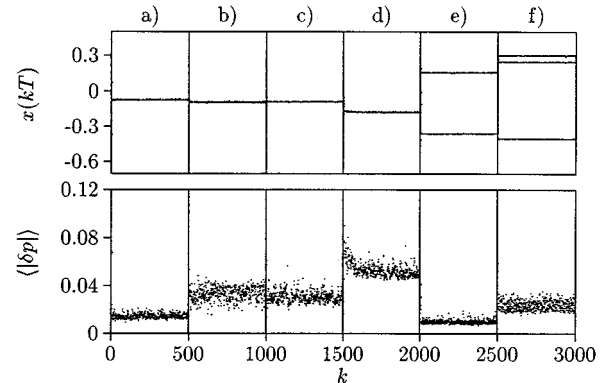

FIG. 9. Local control (modified control requirement) of all UPOs shown in Fig. 3. The magnitude of the unstable eigenvalues of the period-one UPO and of the period-two orbit are of the order 10, while the unstable eigenvalue of the period-three orbit is -720. The control is switched on at $k = 0$; every 500 driving periods we change the UPO to be controlled. The stroboscopic measurement $x(kT)$ in the Poincaré section Σ_1 and the applied control amplitude $\langle |\delta p| \rangle$ averaged over one period of the UPO are shown as functions of the period k.

changes to be taken into account. Here l is the discrete time delay, i.e., $\tau = l\Delta t$, and d the embedding dimension. This is an immediate consequence of the fact that in the time delay embedding space the mapping $\mathbf{P}^{(n,n+1)} = \boldsymbol{\phi}^{\Delta t}_{|\Sigma_n}$ from section Σ_n to the next Σ_{n+1} depends on all preceding parameter values that were changed during the time window $\tau_w = (d-1)\tau$ of the delay vector. In an explicit calculation we show this dependence. In addition, we give a relation between the linearized dynamics in the time-delay embedding space involving A^n and $\mathbf{b}^{n,i}, i = 0, \ldots, w$, and the linearized dynamics $\hat{A}^n$ and $\hat{\mathbf{b}}^n$ in the physical state space. With this relation one can, in principle, calculate A^n and $\mathbf{b}^{n,i}$ from $\hat{A}^n$ and $\hat{\mathbf{b}}^n$ knowing the gradient of the measurement function h. This relation can be exploited in numerical simulations to investigate, e.g., different methods to obtain A^n and $\mathbf{b}^{n,i}$ from measurement data (as we do in Appendix B) or to test quasicontinuous control concepts without the cumbersome extraction of A^n and $\mathbf{b}^{n,i}$ from measurement data.

Starting with the linearized dynamics including A^n and $\mathbf{b}^{n,i}$ in the time-delay space, there are two ways to obtain an explicit control formula. One is the extended state space approach followed by the standard control requirements of the MED and the LC method; the other is a modified control requirement that requires stabilization not for $\mathbf{z}^{n+1}$ but for $\mathbf{z}^{n+w+1}$ with $\delta p^n \neq 0$ and $\delta p^{n+1} = \cdots = \delta p^{n+w} = 0$. With this modified control requirement one bears in mind that the parameter change δp^n influences the system until the section $n+w+1$ and δp^{n-1} only until $n+w$. While for the original OGY method both approaches, i.e., extended state space and modified control requirement, are equivalent, for the quasicontinuous control methods considered here (MED or LC) this is no longer the case. In fact, it turns out that the extended state space approach is not suited for the MED or the LC method as it leads to a control formula that depends on the scaling of the control parameter p. In the experiment we demonstrate that this scaling dependence causes a breakdown of the control for certain units of p. In contrast, the control formulas based on the modified control requirement show a good control performance in the experiment, even for high periodic orbits with large instabilities. Furthermore, between the LC method and the MED method no qualitative difference could be observed. Both methods will lead to satisfying control results provided that a high enough control frequency has been used. Finally, we remark that for control experiments where the control parameters have been determined in advance it is advisable to use an adaptive orbit correction to obtain an optimal reference value for the feedback control. This improves the control performance considerably irrespectively of which OGY control method has been used.

APPENDIX A: EXPLICIT RELATION BETWEEN THE LINEARIZATIONS IN THE PHYSICAL STATE SPACE AND THE DELAY STATE SPACE

In this appendix we show that the linearizations A^n and $\mathbf{b}^{n,i}$ in the time-delay embedding space can be explicitly

calculated from the corresponding linearizations $\hat{A}^n$ and $\hat{\mathbf{b}}^n$ in the physical state space and the gradient of the measurement function h. Before we give this relation we briefly recall our notation of Sec. II. First remember that we always use a caret for the quantities in the physical state space in order to distinguish them from the corresponding ones in the time delay embedding space. The embedding function Φ_n relates a state $\hat{\mathbf{z}}^n$ in the physical state space with a state $\mathbf{z}^n$ in the time delay embedding space. According to Eq. (2), Φ_n depends for active quasicontinuous control on the last w parameter changes, i.e., $\mathbf{z}^n = \Phi_n(\hat{\mathbf{z}}^n, p^{n-w}, \ldots, p^{n-1})$. The vector of parameter perturbation is abbreviated as $\mathbf{p}^{n-1} = (p^{n-w}, \ldots, p^{n-1})$ for active control and for the unperturbed dynamics as $\mathbf{p}_0 = (p_0, \ldots, p_0) \in \mathbb{R}^w$.

Now we can express the relation between the linearizations in the delay state space and the physical state space as

$$A^n = D_{\hat{\mathbf{z}}^n}\Phi_{n+1}(\hat{\mathbf{z}}^{n+1}_F, \mathbf{p}_0) \cdot \hat{A}^n \cdot D_{\hat{\mathbf{z}}^n}\Phi_n(\hat{\mathbf{z}}^n_F, \mathbf{p}_0)^\sharp, \quad \text{(A1a)}$$

$$(\mathbf{b}^{n,w}, \ldots, \mathbf{b}^{n,1}) = N_w \cdot \Gamma_{n+1} - A^n \cdot \Gamma_n, \quad \text{(A1b)}$$

and

$$\mathbf{b}^{n,0} = D_{\hat{\mathbf{z}}^{n+1}}\Phi_{n+1}(\hat{\mathbf{z}}^{n+1}_F, \mathbf{p}_0) \cdot \hat{\mathbf{b}}^n. \quad \text{(A1c)}$$

Here N_w is the $w \times w$ elementary nilpotent block [Eq. (11b)] and $D_{\hat{\mathbf{z}}^n}\Phi_n(\hat{\mathbf{z}}^n_F, \mathbf{p}_0)$ and $\Gamma_n = D_{\mathbf{p}^{n-1}}\Phi_n(\hat{\mathbf{z}}^n_F, \mathbf{p}_0)$ are the Jacobian matrices of Φ_n with respect to the state $\hat{\mathbf{z}}^n$ and the parameter perturbations $\mathbf{p}^{n-1}$. In Eq. (A6) and (A10) these matrices are given as a function of $\hat{A}^n$, $\hat{b}^n$, and the gradient of the measurement function h. Finally, $D_{\hat{\mathbf{z}}^n}\Phi_n(\hat{\mathbf{z}}^n_F, \mathbf{p}_0)^\sharp$ denotes the Penrose pseudoinverse of the $d \times \hat{d}$ matrix $D_{\hat{\mathbf{z}}^n}\Phi_n(\hat{\mathbf{z}}^n_F, \mathbf{p}_0)$ with $\hat{d}$ and d being the dimensions of the Poincaré sections in the physical state space and the delay state space.

In order to derive the relations (A1) we consider the extended states

$$\hat{\mathbf{y}}^n = (\hat{\mathbf{z}}^n, \mathbf{p}^{n-1})^\dagger, \quad \mathbf{y}^n = (\mathbf{z}^n, \mathbf{p}^{n-1})^\dagger$$

and its successors $\hat{\mathbf{y}}^{n+1}$ and $\mathbf{y}^{n+1}$. In the physical state space the flow map $\hat{\mathbf{P}}^{(n,n+1)}$ can be simply extended to a mapping $\hat{\boldsymbol{\mathcal{P}}}^{(n,n+1)}$ that develops a state $\hat{\mathbf{y}}^n$ into $\hat{\mathbf{y}}^{n+1}$ via

$$\hat{\mathbf{y}}^{n+1} = \hat{\boldsymbol{\mathcal{P}}}^{(n,n+1)}(\hat{\mathbf{y}}^n, p^n)$$

$$= (\hat{\mathbf{P}}^{(n,n+1)}(\hat{\mathbf{z}}^n, p^n), \mathbf{p}^n).$$

The linearizations $\hat{C}^n = D_{\hat{\mathbf{y}}}\hat{\boldsymbol{\mathcal{P}}}^{(n,n+1)}(\hat{\mathbf{y}}^n_F, p_0)$ and $\hat{\mathbf{d}}^n = (\partial / \partial p^n)\hat{\boldsymbol{\mathcal{P}}}^{(n,n+1)}(\hat{\mathbf{y}}^n_F, p_0)$ of this map around the UPO $\hat{\mathbf{y}}^n_F = (\hat{\mathbf{z}}^n_F, \mathbf{p}_0)^\dagger$ and p_0 are related to the linearizations of $\hat{\mathbf{P}}^{(n,n+1)}$ in Eq. (5) by

$$\hat{C}^n = \begin{pmatrix} \hat{A}^n & \mathbf{0} \\ \mathbf{0} & N_w \end{pmatrix} \quad \text{(A2a)}$$

and

$$\hat{\mathbf{d}}^n = (\hat{\mathbf{b}}^n, 0, \ldots, 0, 1)^\dagger. \tag{A2b}$$

For the dynamics in the time delay embedding the extended flow map $\mathcal{P}^{(n,n+1)}$ that develops a state $\mathbf{y}^n$ to $\mathbf{y}^{n+1}$ is analogously defined by

$$\mathbf{y}^{n+1} = \mathcal{P}^{(n,n+1)}(\mathbf{y}^n, p^n)$$
$$= (\mathbf{P}^{(n,n+1)}(\mathbf{y}^n, p^n), \mathbf{p}^n). \tag{A3}$$

The linearizations $C^n = D_{\mathbf{y}^n} \mathcal{P}^{(n,n+1)}(\mathbf{y}^n_F, p_0)$ and $\mathbf{d}^n = (\partial/\partial p^n) \mathcal{P}^{(n,n+1)}(\mathbf{y}^n_F, p_0)$ of Eq. (A3) around the embedded UPO $\mathbf{y}^n_F$ and p_0 are already given in Eqs. (10) and (11).

Let us now consider the relation between the mappings $\hat{\mathcal{P}}^{(n,n+1)}$ in the physical state space and $\mathcal{P}^{(n,n+1)}$ in the embedding space. To do this we need the function Ψ_n between the original states $\hat{\mathbf{y}}^n$ and the corresponding states $\mathbf{y}^n$ in the embedding space

$$\mathbf{y}^n = \Psi_n(\hat{\mathbf{y}}^n) = (\Phi_n(\hat{\mathbf{y}}^n), \mathbf{p}^{n-1})^\dagger. \tag{A4}$$

Using this extended embedding functions Ψ_n and writing $\mathcal{P}^{(n,n+1)}_{p^n}$ instead of $\mathcal{P}^{(n,n+1)}(, p^n)$, we obtain

$$\mathcal{P}^{(n,n+1)}_{p^n} = \Psi_{n+1} \circ \hat{\mathcal{P}}^{(n,n+1)}_{p^n} \circ \Psi_n^{-1}.$$

The linearization of this equation leads to a connection between the quantities $\hat{C}^n, \hat{\mathbf{d}}^n$ and $C^n, \mathbf{d}^n$, i.e.,

$$C^n = D_{\hat{\mathbf{y}}^{n+1}} \Psi_{n+1}(\hat{\mathbf{y}}^{n+1}_F) \cdot \hat{C}^n \cdot D_{\mathbf{y}^n} \Psi_n^{-1}(\mathbf{y}^n_F) \tag{A5a}$$

and

$$\mathbf{d}^n = D_{\hat{\mathbf{y}}^{n+1}} \Psi_{n+1}(\hat{\mathbf{y}}^{n+1}_F) \cdot \hat{\mathbf{d}}^n. \tag{A5b}$$

The relations (A5) allow one to calculate the quantities C^n and $\mathbf{d}^n$ from the corresponding linearizations $\hat{C}^n$ and $\hat{\mathbf{d}}^n$ in the physical state space, if $D_{\hat{\mathbf{y}}^{n+1}} \Psi_{n+1}(\hat{\mathbf{y}}^{n+1}_F)$ and $D_{\mathbf{y}^n} \Psi_n^{-1}(\mathbf{y}^n_F)$ are known. As we will demonstrate in the following, it is possible to determine $D_{\hat{\mathbf{y}}^{n+1}} \Psi_{n+1}(\hat{\mathbf{y}}^{n+1}_F)$ and $D_{\mathbf{y}^n} \Psi_n^{-1}(\mathbf{y}^n_F)$ when the linearized flow map $\hat{A}^n$ and $\hat{\mathbf{b}}^n$ in the physical state space and the gradient of the measurement function h are known.

We first consider the embedding function Φ_n defined by Eq. (2) in the case that no control is applied. Let us assume that the physical state space is spanned by the phase of the driving and $\hat{d}$ physical coordinates, so that the Poincaré section $\hat{\Sigma}_n$ is a $\hat{d}$-dimensional set. Having chosen d time-delay coordinates and the phase of the driving for the reconstructed states, the dimension of the standard Poincaré section Σ_n is d, which is in general higher than the dimension $\hat{d}$ of $\hat{\Sigma}_n$ in the physical state space. Therefore, the image of the embedding function $\Phi_n(\hat{\Sigma}_n, \mathbf{p}_0)$ is only a $\hat{d}$-dimensional subset of Σ_n. Restricted to this subset $\Phi_n(, \mathbf{p}_0)$ is a diffeomorphism between $\Phi_n(\hat{\Sigma}_n, \mathbf{p}_0)$ and $\hat{\Sigma}_n$.

Let us now derive the Jacobian matrix $D_{\hat{\mathbf{z}}^n} \Phi_n(\hat{\mathbf{z}}^n_F, \mathbf{p}_0)$ of the embedding function $\Phi_n(, \mathbf{p}_0)$ with respect to a point $\hat{\mathbf{z}}^n_F$. Using the definition of the embedding function in Eq. (2), the entries of the $d \times \hat{d}$ matrix $D_{\hat{\mathbf{z}}^n} \Phi_n(\hat{\mathbf{z}}^n_F, \mathbf{p}_0) = (\phi^n_{i,j})$ are given by

$$\phi^n_{i,j} = \frac{\partial}{\partial \hat{z}^n_j} h(\hat{\mathbf{P}}^{(n,n-(i-1)l)}(\hat{\mathbf{z}}^n_F, \mathbf{p}_0)).$$

The first row of $D_{\hat{\mathbf{z}}^n} \Phi_n(\hat{\mathbf{z}}^n_F, \mathbf{p}_0)$ is the gradient of the measurement function h, i.e., $(\phi^n_{1,1}, \ldots, \phi^n_{1,w}) = \nabla h(\hat{\mathbf{z}}^n_F)$. The remaining entries can be written as

$$\phi^n_{i,j} = [\nabla h \cdot (\hat{A}^{n-(i-1)l})^{-1} \cdots (\hat{A}^{n-1})^{-1}]_j \tag{A6}$$

for $i = 2, \ldots, \hat{d}$, where the square brackets $[\ ]_j$ denote the jth component of the included vector.

Since $\Phi_n(, \mathbf{p}_0)$ maps states from a $\hat{d}$-dimensional space $\hat{\Sigma}_n$ to a subset of the d-dimensional space Σ_n, the inverse of the Jacobian matrix $D_{\hat{\mathbf{z}}^n} \Phi_n(\hat{\mathbf{z}}^n_F, \mathbf{p}_0)$ does not exist. But we can determine the Jacobian matrix of the inverse embedding $\Phi_n^{-1}(, \mathbf{p}_0)$ remembering that $\Phi_n(, \mathbf{p}_0)$ is a diffeomorphism between $\hat{\Sigma}_n$ and the submanifold $\Phi_n(\hat{\Sigma}_n, \mathbf{p}_0)$. Thus the derivative $D_{\hat{\mathbf{z}}^n} \Phi_n(\hat{\mathbf{z}}^n_F, \mathbf{p}_0)$ is bijective between the $\hat{d}$-dimensional tangent spaces $T_{\hat{\mathbf{z}}^n_F} \hat{\Sigma}_n \cong \mathbb{R}^{\hat{d}}$ and $T_{\mathbf{z}^n_F} \Phi_n(\hat{\Sigma}_n, \mathbf{p}_0) \cong \mathbb{R}^{\hat{d}} \subset \mathbb{R}^d$. It is known that in such cases the derivative $D_{\mathbf{z}^n} \Phi_n^{-1}(\mathbf{z}^n_F, \mathbf{p}_0)$ of the inverse mapping $\Phi_n^{-1}(, \mathbf{p}_0)$ with respect to $\mathbf{z}^n_F$ is given by the Penrose pseudoinverse of the matrix $D_{\hat{\mathbf{z}}^n} \Phi_n(\hat{\mathbf{z}}^n_F, \mathbf{p}_0)$. To calculate the pseudoinverse, which we denote by $D_{\hat{\mathbf{z}}^n} \Phi_n(\hat{\mathbf{z}}^n_F, \mathbf{p}_0)^\sharp$, the singular value decomposition of the matrix $D_{\hat{\mathbf{z}}^n} \Phi_n(\hat{\mathbf{z}}^n_F, \mathbf{p}_0)$ can be used. $D_{\hat{\mathbf{z}}^n} \Phi_n(\hat{\mathbf{z}}^n_F, \mathbf{p}_0)^\sharp$ is then given by

$$D_{\hat{\mathbf{z}}^n} \Phi_n(\hat{\mathbf{z}}^n_F, \mathbf{p}_0)^\sharp = V_n \cdot W_n^{-1} \cdot U_n^\dagger, \tag{A7}$$

with $U_n \cdot W_n \cdot V_n^\dagger$ being the singular value decomposition of $D_{\hat{\mathbf{z}}^n} \Phi_n(\hat{\mathbf{z}}^n_F, \mathbf{p}_0)$.

Now we turn to the extended embedding function Ψ_n defined in Eq. (A4), which is used to describe the embedding process when the control is activated. The Jacobian matrix of Eq. (A4) with respect to the point $\hat{\mathbf{y}}^n_F = (\hat{\mathbf{z}}^n_F, \mathbf{p}_0)^\dagger$ is split into four parts

$$D_{\hat{\mathbf{y}}^n} \Psi_n(\hat{\mathbf{y}}^n_F) = \begin{pmatrix} D_{\hat{\mathbf{z}}^n} \Phi_n(\hat{\mathbf{z}}^n_F, \mathbf{p}_0) & \Gamma_n \\ \mathbf{0} & \mathbb{1}_w \end{pmatrix}, \tag{A8}$$

where $\mathbb{1}_w$ is the w-dimensional identity matrix, $\mathbf{0}$ a zero matrix with $\hat{d}$ columns and w rows, and $D_{\hat{\mathbf{z}}^n} \Phi_n(\hat{\mathbf{z}}^n_F, \mathbf{p}_0)$ the above described Jacobian matrix. $\Gamma_n = D_{\mathbf{p}^{n-1}} \Phi_n(\hat{\mathbf{z}}^n_F, \mathbf{p}_0)$ is the Jacobian matrix of Φ_n with respect to the parameter perturbation $\mathbf{p}^{n-1}$ around $\hat{\mathbf{z}}^n_F$ and $\mathbf{p}_0 \in \mathbb{R}^w$. The definition of Φ_n in Eq. (2) leads to a $d \times w$ matrix $\Gamma_n = (\gamma^n_{i,j})$ with

$$\gamma^n_{i,j} = \frac{\partial h (\hat{\mathbf{P}}^{(n,n-(i-1)l)}(\hat{\mathbf{z}}^n_F, p^{n-(i-1)l}, \ldots, p^{n-1}))}{\partial p^{n-w-1+j}}. \tag{A9}$$

All entries $\gamma_{1,j}^n$ in the first row of Γ_n are zero since the first component of $\mathbf{z}^n$ in Eq. (2) does not depend on preceding parameter values. To obtain the second component in Eq. (2) l preceding parameter values are necessary and thus there exist l nonzero entries in the second row of Γ_n. In general, the $\gamma_{i,j}^n$ are nonzero for $i=2,\ldots,d$ and $j=1,\ldots,(i-1)l$. They are given by

$$\gamma_{i,j}^n = \nabla h \cdot (\hat{A}^{n-(i-1)l})^{-1} \cdots (\hat{A}^{n-w-1+j})^{-1} \cdot \hat{\mathbf{b}}^{n-w-1+j}.$$
(A10)

The Jacobian matrix of the inverse embedding process $\Psi_n^{-1}(\mathbf{y}_F^n)$ is now related to the Jacobian matrix $D_{\hat{\mathbf{y}}^n}\Psi_n(\hat{\mathbf{y}}_F^n)$ again via the pseudoinverse $D_{\hat{\mathbf{y}}^n}\Psi_n(\hat{\mathbf{y}}_F^n)^\sharp$. For a numerically stable determination of $D_{\hat{\mathbf{y}}^n}\Psi_n(\hat{\mathbf{y}}_F^n)^\sharp$ it is appropriate to use the relation

$$D_{\hat{\mathbf{y}}^n}\Psi_n(\hat{\mathbf{y}}_F^n)^\sharp = \begin{pmatrix} D_{\hat{\mathbf{z}}^n}\Phi_n(\hat{\mathbf{y}}_F^n)^\sharp & -D_{\hat{\mathbf{z}}^n}\Phi_n(\hat{\mathbf{y}}_F^n)^\sharp \cdot \Gamma_n \\ \mathbf{0} & \mathbb{1}_w \end{pmatrix},$$
(A11)

which follows from Eq. (A8) because the product $D_{\hat{\mathbf{y}}^n}\Psi_n(\hat{\mathbf{y}}_F^n)^\sharp \cdot D_{\hat{\mathbf{y}}^n}\Psi_n(\hat{\mathbf{y}}_F^n)$ gives the identity $\mathbb{1}_{\hat{d}+w}$.

Having determined the quantities $D_{\hat{\mathbf{y}}^n}\Psi_n(\hat{\mathbf{y}}_F^n)$ and $D_{\mathbf{y}^n}\Psi_n^{-1}(\mathbf{y}_F^n) = D_{\hat{\mathbf{y}}^n}\Psi_n(\hat{\mathbf{y}}_F^n)^\sharp$, we finally consider Eq. (A5) once again. Taking into account Eqs. (11), (A2), (A8), and (A11), we obtain the relations given in Eqs. (A1). Having the explicit expressions for Γ_n and $D_{\hat{\mathbf{z}}^{n+1}}\Phi_{n+1}(\hat{\mathbf{z}}_F^{n+1},\mathbf{p}_0)$ [Eqs. (A6) and (A10)] as a function of ∇h, $\hat{A}^n$, and $\hat{\mathbf{b}}^n$ in mind, Eq. (A1) gives an explicit formula to calculate the linearizations in the embedding space.

APPENDIX B: DETERMINATION OF THE LINEARIZATIONS IN THE EMBEDDING SPACE FROM MEASUREMENTS

The relation given in Appendix A can be used to determine the linearizations in a time delay embedding when the corresponding ones in the physical state space are accessible. For example, if the equations of motion are given by an ordinary differential equation then the linearizations $\hat{A}^n$ and $\hat{\mathbf{b}}^n$ can be obtained by numerically integrating the equations of motion together with its variational equations [22]. With the relation of Appendix A, the linearizations A^n and $\mathbf{b}^{n,i}$ in the embedding space can then easily be calculated. Usually in experiments the equations of motion are not known and thus the linearizations have to be determined solely from experimental data. We will now show how we extract the linearizations A^n and $\mathbf{b}^{n,i}$ from two time series.

For that purpose we consider a numerical simulation of a Duffing oscillator so that we are able to compare the linearizations extracted from a time series with the correct ones. The double-well Duffing oscillator is given by $\ddot{x} + \alpha\dot{x} - x + x^3 = \gamma\cos\omega t + p$, with $\alpha=0.15$, $\gamma=0.3$, and $\omega=1$ [23]. According to our notation, a point in the standard Poincaré section $\overset{\circ}{\Sigma}_n$ is given by $\hat{\mathbf{z}}^n = (x(t_0+n\Delta t),\dot{x}(t_0+n\Delta t))^\dagger$, with $\Delta t=T/N$. As in the bronze ribbon experiment, we use $N=64$ Poincaré sections.

An UPO $\hat{\mathbf{z}}_F^n$ of the system has been determined by a standard Newton algorithm and the corresponding linearizations $\hat{A}^n$ and $\hat{\mathbf{b}}^n$ via the variational equations. As the measurement function h we use the displacement of the oscillator, i.e., $h(\hat{\mathbf{z}}^n) = x^n = x(t_0+n\Delta t)$. The dynamics of the system is reconstructed with $d=3$ time delay cooordinates and a delay $l=10$. The values $d=3$ and $\tau=10\Delta t$ are obtained by the integral local deformation method of Buzug and Pfister [20].

To extract the mappings A^n we numerically integrate the system 100 000 periods and record in each section Σ_n $m=100$ nearest-neighbor points $\mathbf{z}^{nj}$ of $\mathbf{z}_F^n$ and the following points $\mathbf{z}^{nj+1}$. In a first attempt one may try to estimate the mappings A^n from a least-squares fit using the relation

$$\delta\mathbf{z}^{nj+1} = A^n \cdot \delta\mathbf{z}^{nj},$$
(B1)

with $\delta\mathbf{z}^{nj+1} = \mathbf{z}^{nj+1} - \mathbf{z}_F^{n+1}$ and $\delta\mathbf{z}^{nj} = \mathbf{z}^{nj} - \mathbf{z}_F^n$. To realize that this attempt is not optimal, we remember that the mappings A^n, which are represented by $d\times d$ matrices, describe the linearization of the dynamics from the $\hat{d}$-dimensional tangent spaces $T_{\mathbf{z}_F^n}\Phi_n(\overset{\circ}{\Sigma}_n,\mathbf{p}_0)$ embedded in $\mathbb{R}^d$ to the tangent spaces $T_{\mathbf{z}_F^{n+1}}\Phi_{n+1}(\overset{\circ}{\Sigma}_{n+1},\mathbf{p}_0)$ embedded in $\mathbb{R}^d$. Thus, for an optimal estimation it is necessary that the difference vectors $\delta\mathbf{z}_j^n$ and $\delta\mathbf{z}^{nj+1}$ lie in the tangent space $T_{\mathbf{z}_F^n}\Phi_n(\overset{\circ}{\Sigma}_n,\mathbf{p}_0)$ and $T_{\mathbf{z}_F^{n+1}}\Phi_{n+1}(\overset{\circ}{\Sigma}_{n+1},\mathbf{p}_0)$, respectively. But, in general, the $\delta\mathbf{z}^{nj}$ are not infinitesimal and the $\mathbf{z}^{nj}$ and $\mathbf{z}^{nj+1}$ lie in $\Phi_n(\overset{\circ}{\Sigma}_n,\mathbf{p}_0)$ and $\Phi_{n+1}(\overset{\circ}{\Sigma}_{n+1},\mathbf{p}_0)$, which generally have a curvature in Σ_n and Σ_{n+1}. Therefore, $\delta\mathbf{z}^{nj}$ and $\delta\mathbf{z}^{nj+1}$ of the m nearest-neighbor points are not restricted to a $\hat{d}$-dimensional subspace as they should be in the ideal case of inifinitesimal distances.

To eliminate these extra dimensions that enter due to the curvature of $\Phi_n(\overset{\circ}{\Sigma}_n,\mathbf{p}_0)$ and $\Phi_{n+1}(\overset{\circ}{\Sigma}_{n+1},\mathbf{p}_0)$ we introduce projections $\Pi_{\mathbf{z}_F^n}$ and $\Pi_{\mathbf{z}_F^{n+1}}$ that project the differences $\delta\mathbf{z}^{nj}$ and $\delta\mathbf{z}^{nj+1}$ onto the corresponding tangent spaces. The projection $\Pi_{\mathbf{z}_F^n}$ can be estimated using the singular value decomposition $U_n \cdot W_n \cdot V_n^\dagger$ of the matrix $(\delta\mathbf{z}^{n1},\ldots,\delta\mathbf{z}^{nm})^\dagger$ of nearest neighbors of $\mathbf{z}_F^n$. The singular values of this matrix measure the extension of the nearest-neighbor points in the direction of the corresponding singular vectors, which are the columns of the orthogonal matrix V_n. Assuming a sufficiently small neighborhood, the nearest-neighbor points are mainly spread in the direction of the tangent space. Thus the tangent space is spanned by the directions corresponding to the $\hat{d}$ largest singular values, where $\hat{d}$ is the dimension of the tangent space $T_{\mathbf{z}_F^n}\Phi_n(\overset{\circ}{\Sigma}_n,\mathbf{p}_0)$. The remaining singular vectors are normal to the tangent space, indicating the directions of the curvature of the manifold. So we obtain for the projections

$$\Pi_{\mathbf{z}_F^n} = V_n \cdot \mathrm{diag}(\underbrace{1,\ldots,1}_{\hat{d}},0,\ldots,0) \cdot V_n^\dagger,$$

assuming that the singular values are ordered by size. In the case that the dimension $\hat{d}$ of the tangent space is not known the method proposed in [24,25] can be used to estimate $\hat{d}$. Broomhead, Jones, and King show that the directions of the
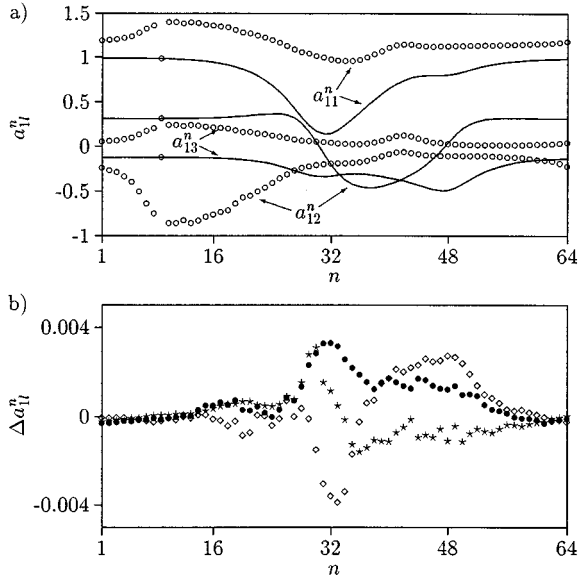
FIG. 10. (a) First row (a_{1l}^n) of the linearizations A^n versus $n = 1, \ldots, N = 64$ for an UPO of the Duffing oscillator using $d = 3$ time-delay coordinates with time delay $\tau = 10/64T$. The solid lines indicate the numerically calculated values [variational equations and relation (A1a)] and the circles the values obtained by a least-squares fit using Eq. (B1). (b) The differences $\Delta a_{1l}^n = a_{1l,\text{fit}}^n - a_{1l,\text{correct}}^n$ of the numerically calculated A^n and the ones obtained from a least-squares fit using the projections in Eq. (B2) are shown for the components $l = 1$ ($\diamond$), $l = 2$ ($\star$), and $l = 3$ ($\bullet$).

tangent space can be identified by the scaling behavior of the corresponding singular values when the diameter of the neighborhood is decreased.

After the determination of the projections, the mapping A^n is estimated using the relation

$$\Pi_{\mathbf{z}_F^{n+1}} \cdot \delta \mathbf{z}^{n_j+1} = A^n \cdot \Pi_{\mathbf{z}_F^n} \cdot \delta \mathbf{z}^{n_j} \qquad (B2)$$

instead of Eq. (B1). We investigated with the numerical simulation of the Duffing oscillator the effect of using the fit (B2) instead of Eq. (B1). In Fig. 10(a) we show the first row of A^n versus n resulting from a least-squares fit using Eq. (B1) and from a numerical calculation using the variational equations and the relation (1a). As can be seen, the values of A^n differ substantially. This error results from the neglected curvature of the nearest-neighbor points. In contrast to this, in Fig. 10(b) we plot the differences of the first row of the numerically calculated A^n with the one obtained by using Eq. (B2) for the fit. The maximal error is less than 0.004, so the
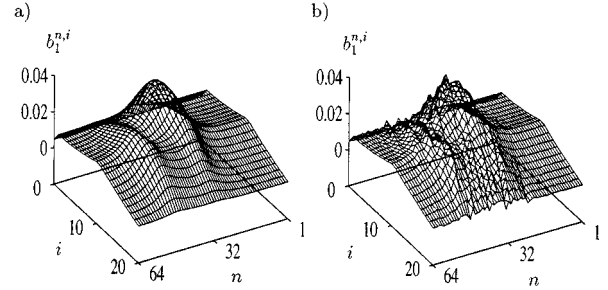

FIG. 11. For an UPO of the Duffing oscillator the first component $b_1^{n,i}$ of the dependences $\mathbf{b}^{n,i}$, $i = 0, \ldots, w = 20$, and $n = 1, \ldots, N = 64$ is shown: (a) numerically calculated ones using Eqs. (A1b) and (A1c) and (b) extracted ones using the least-squares fit (B3).

components of A^n using Eq. (B2) could not be distinguished from the solid line of the numerically calculated ones if they were plotted in Fig. 10(a) too. This demonstrates that the use of the projections in Eq. (B2) is necessary to improve the estimation of the mappings A^n from a time series analysis.

In addition to the matrices A^n, the dependences $\mathbf{b}^{n,i}$ on the control parameter have to be extracted from the analysis of the experimental data. To do this the system is disturbed every Δt by a small random parameter perturbation δp^n. The resulting time series then consists of a set of data pairs

$$(x^1, \delta p^1), (x^2, \delta p^2), (x^3, \delta p^3), \ldots .$$

Once again, out of 100 000 periods we record in each section Σ_n $m = 300$ nearest-neighbor points $\mathbf{z}^{n_j}$ of $\mathbf{z}_F^n$ and the successor points $\mathbf{z}^{n_j+1}$. Since the dynamics A^n of the system in the neighborhood of the UPO has already been determined we use the difference between a vector $\delta \mathbf{z}^{n_j+1}$ and $A^n \cdot \delta \mathbf{z}^{n_j}$ to determine the dependences $\mathbf{b}^{n,w}, \ldots, \mathbf{b}^{n,0}$. They are obtained by a least-squares fit using

$$\Pi_{\mathbf{z}_F^{n+1}} \cdot (\delta \mathbf{z}^{n_j+1} - A^n \cdot \delta \mathbf{z}^{n_j}) = \sum_{i=0}^{w} \mathbf{b}^{n,i} \delta p^{n_j-i}. \qquad (B3)$$

The projection $\Pi_{\mathbf{z}_F^{n+1}}$ is used for the same reason as in Eq. (B2).

The successful determination of the dependences $\mathbf{b}^{n,i}$ is exemplarily demonstrated for the UPO of the Duffing oscillator. Both the numerically calculated first component of $\mathbf{b}^{n,i}$ and the corresponding values extracted from a perturbed time series are shown in Fig. 11. The agreement between the exact values and the values extracted from a time series is clearly visible, but it is not as good as in Fig. 10 where the mapping A^n has been determined.

[1] A. Hübler and E. Lüscher, Naturwissenschaften **76**, 67 (1989).

[2] E. Ott, C. Grebogi, and J.A. Yorke, Phys. Rev. Lett. **64**, 1196 (1990).

[3] T. Shinbrot, C. Grebogi, E. Ott, and J.A. Yorke, Nature **363**, 411 (1993).

[4] I.B. Schwartz and I. Triandaf, Phys. Rev. A **46**, 7439 (1992).

[5] E.R. Hunt, Phys. Rev. Lett. **67**, 1953 (1991).

[6] C. Reyl, L. Flepp, R. Badii, and E. Brun, Phys. Rev. E **47**, 267 (1993).

[7] B. Hübinger, R. Doerner, and W. Martienssen, Z. Phys. B **90**, 103 (1993).

[8] B. Hübinger, R. Doerner, W. Martienssen, M. Herdering, R. Pitka, and U. Dressler, Phys. Rev. E **50**, 932 (1994).

[9] N.H. Packard, J.P. Crutchfield, J.D. Farmer, and R.S. Shaw,

Phys. Rev. Lett. **45**, 712 (1980).

[10] F. Takens, in *Dynamical Systems and Turbulence*, edited by D. Rand and L.S. Young (Springer, Berlin, 1981).

[11] T. Sauer, J.A. Yorke, and M. Casdagli, J. Stat. Phys. **65**, 579 (1991).

[12] U. Dressler and G. Nitsche, Phys. Rev. Lett. **68**, 1 (1992).

[13] F.J. Romeiras, C. Grebogi, E. Ott, and W.P. Dayawansa, Physica D **58**, 165 (1992).

[14] P. So and E. Ott, Phys. Rev. E **51**, 2955 (1995).

[15] M. Ding, W. Yang, V. In, W.L. Ditto, M.L. Spano, and B. Gluckman, Phys. Rev. E **53**, 4334 (1996).

[16] R. Doerner, B. Hübinger, and W. Martienssen, Int. J. Bif. Chaos **5**, 1175 (1995).

[17] R.J. de Korte, J.C. Schouten, and C.M. van den Bleek, Phys. Rev. E **52**, 3358 (1995).

[18] G. Nitsche and U. Dressler, Physica D **58**, 153 (1992).

[19] F.C. Moon, *Chaotic Vibrations* (Wiley, New York, 1987).

[20] Th. Buzug and G. Pfister, Phys. Rev. A **45**, 7073 (1992).

[21] U. Dressler, T. Ritz, A. Schenck zu Schweinsberg, R. Doerner, B. Hübinger, and W. Martienssen, Phys. Rev. E **51**, 1845 (1995).

[22] J.-P. Eckmann and D. Ruelle, Rev. Mod. Phys **57**, 617 (1985).

[23] J. Guckenheimer and P. Holmes, *Nonlinear Oscillations, Dynamical Systems and Bifurcations of Vector Fields* (Springer, New York, 1983).

[24] D.S. Broomhead, R. Jones, and P. King, J. Phys. A **20**, L563 (1987).

[25] D.S. Broomhead and R. Jones, Proc. R. Soc. London Ser. A **423**, 103 (1989).